

Discovery of interstellar NC_4NH^+ : dicyanopolyynes are indeed abundant in space[★]

M. Agúndez¹, C. Cabezas¹, N. Marcelino^{2,3}, R. Fuentetaja¹, B. Tercero^{2,3}, P. de Vicente³, and J. Cernicharo¹

¹ Instituto de Física Fundamental, CSIC, Calle Serrano 123, E-28006 Madrid, Spain
e-mail: marcelino.agundez@csic.es, jose.cernicharo@csic.es

² Observatorio Astronómico Nacional, IGN, Calle Alfonso XII 3, E-28014 Madrid, Spain

³ Observatorio de Yebes, IGN, Cerro de la Palera s/n, E-19141 Yebes, Guadalajara, Spain

Received; accepted

ABSTRACT

The previous detection of two species related to the non polar molecule cyanogen (NCCN), its protonated form (NCCNH^+) and one metastable isomer (CNCN), in cold dense clouds supported the hypothesis that dicyanopolyynes are abundant in space. Here we report the first identification in space of NC_4NH^+ , which is the protonated form of NC_4N , the second member of the series of dicyanopolyynes after NCCN . The detection was based on the observation of six harmonically related lines within the Yebes 40m line survey of TMC-1 QUIJOTE. The six lines can be fitted to a rotational constant $B = 1293.90840 \pm 0.00060$ MHz and a centrifugal distortion constant $D = 28.59 \pm 1.21$ Hz. We confidently assign this series of lines to NC_4NH^+ based on high-level ab initio calculations, which supports the previous identification of HC_5NH^+ by Marcelino et al. (2020) from the observation of a series of lines with a rotational constant 2 MHz lower than that derived here. The column density of NC_4NH^+ in TMC-1 is $(1.1_{-0.6}^{+1.4}) \times 10^{10}$ cm^{-2} , which implies that NC_4NH^+ is eight times less abundant than NCCNH^+ . The species CNCN , previously reported toward L483 and tentatively in TMC-1, is confirmed in this latter source. We estimate that NCCN and NC_4N are present in TMC-1 with abundances a few times to one order of magnitude lower than HC_3N and HC_5N , respectively. This means that dicyanopolyynes $\text{NC}-(\text{CC})_n-\text{CN}$ are present at a lower level than the corresponding monocyano polyynes $\text{HCC}-(\text{CC})_n-\text{CN}$. The reactions of the radicals CN and C_3N with HNC arise as the most likely formation pathways to NCCN and NC_4N in cold dense clouds.

Key words. astrochemistry – line: identification – molecular processes – ISM: molecules – radio lines: ISM

1. Introduction

Dicyanopolyynes are molecules with a linear unsaturated skeleton of carbon atoms terminated at each edge by a cyano group, that is, $\text{N}\equiv\text{C}-(\text{C}\equiv\text{C})_n-\text{C}\equiv\text{N}$. The simplest member of this family, cyanogen (NCCN), has been long known to be present in the atmosphere of Titan (Kunde et al. 1981; Coustenis et al. 1991; Sylvestre et al. 2020) and has been recently identified in the coma of comet 67P/Churyumov-Gerasimenko (Hänni et al. 2021). The second member of the series, dicyanoacetylene (NC_4N), has been observed in solid state, although not in the gas phase, in the atmosphere of Titan (Samuelson et al. 1997; Jolly et al. 2015). It is also interesting to note that NCCP , a species chemically related to NCCN that results from the substitution of one N atom by one P atom, has been identified tentatively in the carbon star envelope IRC +10216 (Agúndez et al. 2014).

It has been hypothesized that dicyanopolyynes could be abundant in interstellar and circumstellar clouds (Kołos & Grabowski 2000; Petrie et al. 2003). Indeed, it is well known that monocyano polyynes, more commonly known as cyanopolyynes, i.e., $\text{H}-\text{C}\equiv\text{C}-(\text{C}\equiv\text{C})_n-\text{C}\equiv\text{N}$, are abundant in cold dense clouds and circumstellar envelopes around evolved stars, and thus it is conceivable that dicyanopolyynes are abundant as well. How-

ever, dicyanopolyynes are non polar and thus cannot be detected at radio wavelengths. In spite of that, in recent years we learnt that dicyanopolyynes are very likely abundant in interstellar clouds. The protonated form of cyanogen, NCCNH^+ , was detected in the cold dense clouds TMC-1 and L483 (Agúndez et al. 2015). Just as N_2H^+ is used to probe N_2 (Linke et al. 1983), the detection of NCCNH^+ was interpreted as an indirect evidence of the presence of NCCN , for which a large abundance, in the range $(1-10) \times 10^{-8}$ relative to H_2 , was inferred. A second piece of evidence in support of the presence of cyanogen in interstellar clouds was provided by the detection of isocyanogen (CNCN) in the cold dense clouds L483, TMC-1 (tentatively), and L1544 (Agúndez et al. 2018; Vastel et al. 2019). This species is a polar metastable isomer of NCCN , and thus it is very likely chemically connected to cyanogen. From the detection of CNCN , Agúndez et al. (2018) inferred an abundance of NCCN in the range $(2.5-4.5) \times 10^{-9}$ relative to H_2 .

Here we present an additional evidence in support of the existence of abundant dicyanopolyynes in the interstellar medium. We identified a series of six harmonically related lines in the QUIJOTE¹ line survey of TMC-1 (Cernicharo et al. 2021c, 2022b), which are convincingly assigned to NC_4NH^+ . This is the protonated form of dicyanoacetylene (NC_4N), and thus indirectly probes the presence of the second member of the family of dicyanopolyynes. We discuss how abundant are likely to be in-

[★] Based on observations carried out with the Yebes 40m telescope (projects 19A003, 20A014, 20D023, 21A011, and 21D005). The 40m radio telescope at Yebes Observatory is operated by the Spanish Geographic Institute (IGN; Ministerio de Transportes, Movilidad y Agenda Urbana).

¹ Q-band Ultrasensitive Inspection Journey to the Obscure TMC-1 Environment.

terstellar dicyanopolyynes in comparison with their monocyano counterparts.

2. Observations

The observational data used here is based on QUIJOTE (Cernicharo et al. 2021c, 2022b), an ongoing line survey that is being carried out with the Yebes 40m telescope at the position of the cyanopolyne peak of TMC-1, $\alpha_{J2000} = 4^{\text{h}}41^{\text{m}}41.9^{\text{s}}$ and $\delta_{J2000} = +25^{\circ}41'27.0''$. QUIJOTE uses a 7 mm receiver covering the Q band (31.0-50.3 GHz) with horizontal and vertical polarizations. The backend is a fast Fourier transform spectrometer providing a spectral resolution of 38.15 kHz and a bandwidth of 8×2.5 GHz in each polarization, which allows to cover almost completely the whole Q band. The system is described by Tercero et al. (2021). The data presented here were acquired from November 2019 to May 2022 using the frequency-switching technique, and comprise 546 h of on-source telescope time. The intensity scale used is antenna temperature, T_A^* , which has an estimated uncertainty of 10 % and can be converted to main beam brightness temperature, T_{mb} , by dividing by $B_{\text{eff}}/F_{\text{eff}}$, where B_{eff} and F_{eff} are the beam and forward efficiencies, respectively. For the Yebes 40m telescope in the Q band², $F_{\text{eff}} = 0.97$ and B_{eff} can be fitted as a function of frequency as $B_{\text{eff}} = 0.797 \exp[-(\nu(\text{GHz})/71.1)^2]$, where the expression corresponds to values measured during 2022 that represent a slight improvement over previous values due to a better alignment of mirrors in the receiver cabin. The half power beam width (HPBW) can also be fitted as a function of frequency as $\text{HPBW}('') = 1763/\nu(\text{GHz})$. Some spectra of TMC-1 presented in Sec. 4 were observed with the IRAM 30m telescope. These observations are described in Cabezas et al. (2022a). All data were analyzed using the GILDAS software³.

3. Results

3.1. Identification of NC_4NH^+

We identified six lines in the QUIJOTE line survey whose frequencies show harmonic relations 13/14/15/16/17/18. Multiples of these relations are not possible because lines corresponding to their intermediate frequencies with similar intensities are missing. We could not assign these lines to any molecule with known rotational spectroscopy, after inspection of the private catalog of J. Cernicharo MADEX⁴ (Cernicharo 2012), the Cologne Database for Molecular Spectroscopy (CDMS)⁵ (Müller et al. 2005), and the Jet Propulsion Laboratory (JPL) catalog⁶ (Pickett et al. 1998). The six lines are weak, with intensities around 1 mK in T_A^* . However, given the T_A^* noise level reached by the QUIJOTE data, in the range 0.1-0.2 mK at frequencies below 45 GHz, most of the lines are detected with a high signal-to-noise ratio. The lines are shown in Fig. 1 and the frequencies measured, together with the rest of line parameters derived from a Gaussian fit, are given in Table 1.

The line frequencies can be fitted as $\nu(J \rightarrow J-1) = 2BJ - 4DJ^3$, yielding a rotational constant $B = 1293.90840 \pm 0.00060$ MHz and a centrifugal distortion constant $D = 28.59 \pm 1.21$ Hz, with a rms of 13.5 kHz (see Table 2). The six lines show a nearly perfect harmonic relation and have similar intensities. Moreover,

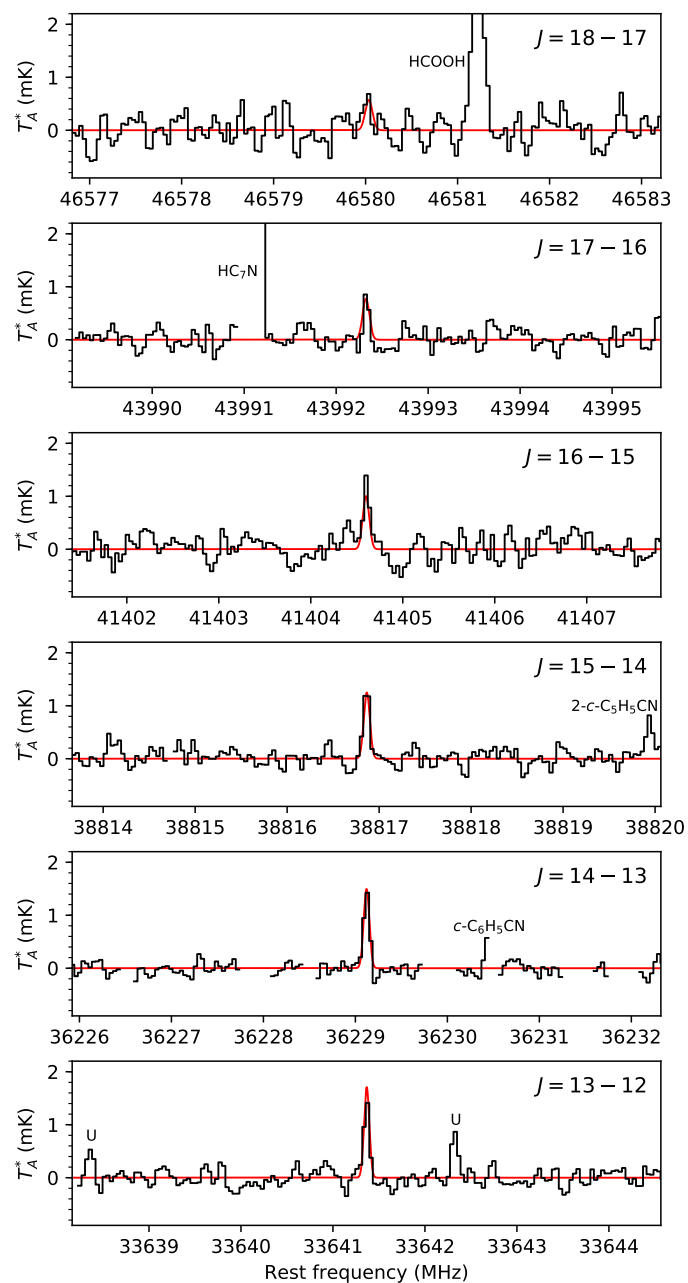


Fig. 1. Lines of NC_4NH^+ observed toward TMC-1. Blanked channels correspond to negative artifacts resulting from the frequency switching observing mode. Unidentified lines are labeled as "U". The red lines correspond to the line profiles calculated under LTE adopting a column density of $1.2 \times 10^{10} \text{ cm}^{-2}$, a rotational temperature of 5.6 K, a linewidth of 0.60 km s^{-1} , and an emission size of $40''$ in radius (see text).

there is no missing line that should be detected and it is not. For example, the $J = 12-11$ line, predicted at 31053.604 MHz, lies outside the frequency range covered and the $J = 19-18$ line, predicted at 49167.735 MHz and expected with an intensity of $T_A^* \sim 0.4$ mK, is not detected because the T_A^* noise level in this frequency range is at the level of 0.3 mK. Given these facts, it is extremely unlikely that the six lines do not arise from the same carrier.

The rotational constant B derived here matches very well the theoretical rotational constant calculated for protonated dicyanoacetylene (NC_4NH^+), 1293.54 MHz (Marcelino et al. 2020). This value was calculated ab initio and scaled using the

² https://rt40m.oan.es/rt40m_en.php

³ <http://www.iram.fr/IRAMFR/GILDAS/>

⁴ https://nanocosmos.iff.csic.es/?page_id=1619

⁵ <https://cdms.astro.uni-koeln.de/>

⁶ <https://spec.jpl.nasa.gov/>

Table 1. Observed line parameters of NC₄NH⁺ in TMC-1.

Transition	ν_{obs}^a (MHz)	$\nu_{obs} - \nu_{calc}^b$ (MHz)	$\Delta\nu^c$ (km s ⁻¹)	T_A^* peak (mK)	$\int T_A^* dv$ (mK km s ⁻¹)
$J = 13-12$	33641.365 ± 0.010	-0.002	0.64 ± 0.11	1.48 ± 0.13	1.01 ± 0.14
$J = 14-13$	36229.121 ± 0.010	+0.000	0.61 ± 0.14	1.49 ± 0.11	0.96 ± 0.20
$J = 15-14$	38816.863 ± 0.010	-0.003	0.61 ± 0.07	1.39 ± 0.13	0.90 ± 0.09
$J = 16-15$	41404.606 ± 0.010	+0.006	0.61 ± 0.15	1.33 ± 0.20	0.86 ± 0.16
$J = 17-16$	43992.330 ± 0.010	+0.006	0.37 ± 0.12	1.00 ± 0.16	0.40 ± 0.08
$J = 18-17$	46580.010 ± 0.020	-0.025	0.62 ± 0.28	0.64 ± 0.25	0.42 ± 0.16

The line parameters ν_{obs} , $\Delta\nu$, T_A^* peak, and $\int T_A^* dv$ as well as the associated errors were derived from a Gaussian fit to each line profile. ^a Observed frequencies adopting a systemic velocity of 5.83 km s⁻¹ for TMC-1 (Cernicharo et al. 2020a). ^b Observed minus calculated frequencies, where calculated frequencies, ν_{calc} , are computed using $B = 1293.90840$ MHz and $D = 28.60$ Hz (see text). ^c $\Delta\nu$ is the full width at half maximum.

Table 2. Spectroscopic parameters of NC₄NH⁺.

Parameter	Astronomical ^a	Theoretical ^b
B (MHz)	1293.90840(60)	1293.54
D (Hz)	28.59(121)	27.8
rms (kHz)	13.5	
μ (D)		9.1

Numbers in parentheses are 1 σ uncertainties in units of the last digits. ^a Values derived from a fit to the frequencies observed in TMC-1. The rms is the standard deviation of the fit. ^b Calculated values reported in Marcelino et al. (2020). The dipole moment is calculated at the MP2/cc-pVTZ level.

experimental-to-calculated ratio of B for NC₄N, a method that has been used previously to detect molecules such as HC₃O⁺ (Cernicharo et al. 2020b), HC₃S⁺ (Cernicharo et al. 2021a), CH₃CO⁺ (Cernicharo et al. 2021b), H₂NC (Cabezas et al. 2021), HCCS⁺ (Cabezas et al. 2022a), C₃H⁺ (Cernicharo et al. 2022a), HC₇NH⁺ (Cabezas et al. 2022b), and HCCNCH⁺ (Agúndez et al. 2022). In all these cases the difference between calculated and astronomical rotational constant was below 0.1 %, and for HC₃O⁺, HC₃S⁺, and CH₃CO⁺ the identification was definitively confirmed by laboratory spectra. Here, the difference between the calculated rotational constant of NC₄NH⁺ and the astronomical value derived from the six lines observed in TMC-1 is 0.03 %. The centrifugal distortion constant calculated for NC₄NH⁺ by Marcelino et al. (2020), 27.8 Hz, is also very close to the value derived from the astronomical lines (see Table 2).

Other potential candidates, apart from NC₄NH⁺, are HC₅O⁺ and HC₅NH⁺, as discussed by Marcelino et al. (2020). It is unlikely that HC₅O⁺ is the carrier because its calculated rotational constant is significantly different, by 0.7 %, from that derived here. The rotational constants calculated for NC₄NH⁺ and HC₅NH⁺ are close, although all levels of theory predict a rotational constant 2 MHz larger for HC₅NH⁺ than for NC₄NH⁺, which is consistent with the assignment of the series of lines observed here to NC₄NH⁺ and that observed by Marcelino et al. (2020) to HC₅NH⁺. In addition, if this is the case, the differences between the calculated and the astronomical rotational constant for NC₄NH⁺ and HC₅NH⁺ remain small, 0.03 % and 0.02 %, respectively, while if the assignment was the reverse, the differences would be significantly larger, 0.18 % and 0.12 %, respectively. That is, we conclude that the identification of HC₅NH⁺ presented by Marcelino et al. (2020) is correct and that the series of harmonically related lines presented here correspond to NC₄NH⁺. The excitation of the two molecules is in line with the

assignment made (see Sec. 3.2), which in any case will require of laboratory measurements for a definitive confirmation.

3.2. Abundance of NC₄NH⁺

To evaluate how abundant is NC₄NH⁺ in TMC-1 we adopt a dipole moment of 9.1 D, as calculated at the MP2/cc-pVTZ level by Marcelino et al. (2020). These authors calculated slightly higher values, in the range 9.5-9.9 D, using coupled cluster methods, although the MP2 level of theory yields probably a more accurate estimation of the dipole moment of NC₄NH⁺, as suggested by the case of HC₅N investigated in Marcelino et al. (2020).

Using the velocity-integrated line intensities given in Table 1, we constructed a rotation diagram, which is shown in the left panel of Fig. 2. We assumed that the emission of NC₄NH⁺ is distributed in the sky as a circle with a diameter of 80'', as observed for several hydrocarbons in TMC-1 (Fossé et al. 2001). We derived a rotational temperature of 6.1 ± 1.4 K, which is in the range of the rotational temperatures derived for other molecules observed in TMC-1, between 5 and 10 K. The column density derived from the rotation diagram is $(1.1 \pm 0.9) \times 10^{10}$ cm⁻². In order to get rid of some of the assumptions made by the rotation diagram method, such as the validity of the Rayleigh-Jeans limit, we carried out calculations assuming local thermodynamic equilibrium (LTE), with a single rotational temperature governing the excitation of all rotational levels, in which the rotational temperature and column density were varied. The best fit is then given by the minimum χ^2 , defined as $\chi^2 = \sum [(I_{calc} - I_{obs})/\sigma]^2$, where the sum extends over the six lines, I_{calc} and I_{obs} are the calculated and observed velocity-integrated intensities, and σ is the error in I_{obs} . In the right panel of Fig. 2 we plot χ^2 as a function of the rotational temperature and the column density. The best fit values of the rotational temperature and column density found this way are 5.6 ± 1.9 K and $(1.1^{+1.4}_{-0.6}) \times 10^{10}$ cm⁻², which should be more precise than the values obtained through the rotation diagram method. In any case, the differences are small and only affect the rotational temperature since the column densities obtained through the two methods are identical. The calculated line profiles using these best fit parameters are shown in Fig. 1.

By comparing the rotational temperature derived here for NC₄NH⁺, 5.6 ± 1.9 K, with that derived for HC₅NH⁺, 7.8 ± 0.7 K (Marcelino et al. 2020), we can find an additional argument in support of the assignment to NC₄NH⁺ made here. That is, the fact that the rotational temperature of NC₄NH⁺ is smaller than for HC₅NH⁺ is consistent with the higher dipole moment

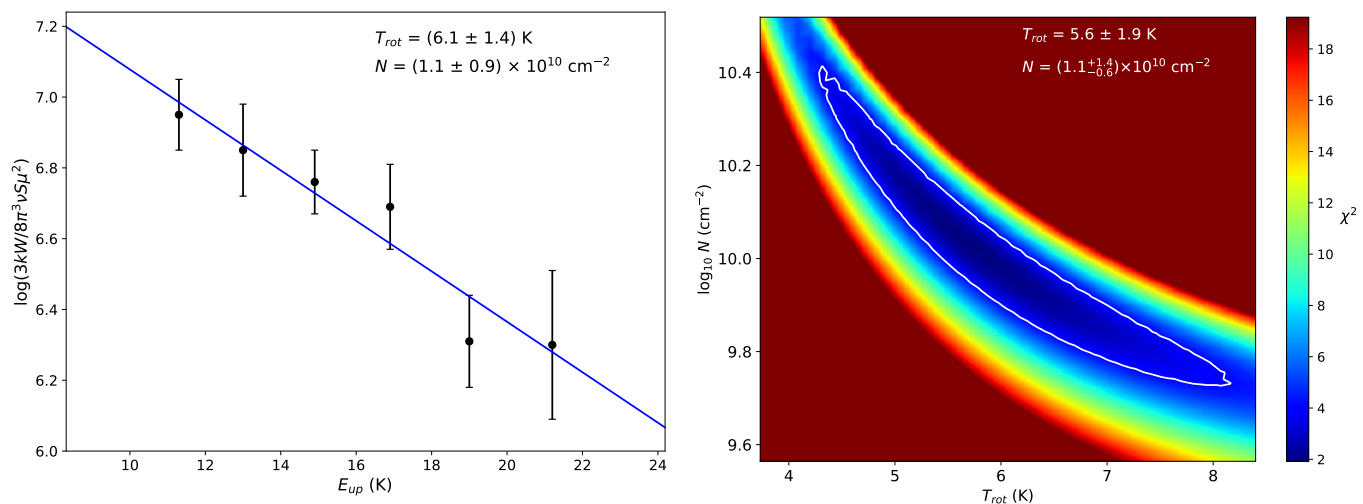


Fig. 2. Excitation analysis of NC_4NH^+ in TMC-1. In the left panel we show the rotation diagram and in the right panel we show the χ^2 resulting from a LTE calculation, where the contour corresponds to the 1σ level. The rotational temperature and column density derived through the two methods are very similar.

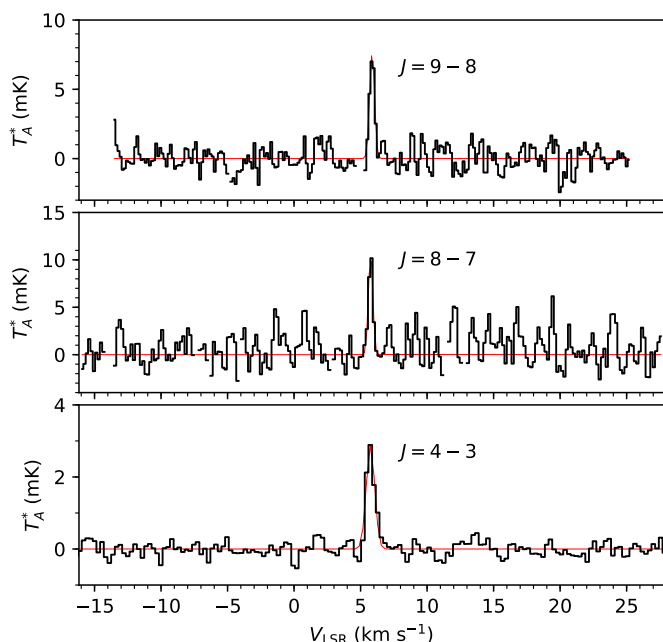


Fig. 3. Lines of CNCN observed toward TMC-1. In red we show the Gaussian fits, which yield $\int T_A^* dv$ (in mK km s $^{-1}$) of 2.27 ± 0.13 , 4.47 ± 0.75 , and 3.55 ± 0.33 for the $J=4-3$, $J=8-7$, and $J=9-8$ lines, respectively.

of NC_4NH^+ compared to that of HC_5NH^+ , 9.1 D versus 3.6 D (Marcelino et al. 2020), because the larger the dipole moment, the larger is the critical density for thermalization, and the lower the value of the rotational temperature.

4. Discussion

Just as the detection of NCCNH^+ and CNCN (Agúndez et al. 2015, 2018) provided indirect evidence on the existence of the highly stable, but non polar, molecule NCCN in cold dense clouds, the detection of NC_4NH^+ reported here provides indirect evidence on the presence of the non polar molecule NC_4N .

In the case of cyanogen (NCCN), there are two indirect proxies: the protonated form NCCNH^+ and the metastable isomer CNCN . The column density of NCCNH^+ in TMC-1 is 8.6×10^{10} cm $^{-2}$ (Agúndez et al. 2015), while for CNCN the detection in TMC-1 presented by Agúndez et al. (2018) was based on line stacking of four lines in the λ 3 mm band and was therefore considered only as tentative. Here we present the confirmation of the detection of CNCN in TMC-1 thanks to the clear detection of three lines (see Fig. 3): the $J=4-3$ line at 41392.912 MHz in our QUIJOTE data and the $J=8-7$ and $J=9-8$ lines at 82784.692 MHz and 93132.326 MHz, respectively, using IRAM 30m data (observations are described in Cabezas et al. 2022a). We derive a rotational temperature of 10.6 ± 1.6 K and a column density of $(8.0 \pm 2.1) \times 10^{11}$ cm $^{-2}$, which is similar to the value of 9×10^{11} cm $^{-2}$ derived by Agúndez et al. (2018). Therefore, the abundance ratio $\text{CNCN}/\text{NCCNH}^+$ in TMC-1 is ~ 9 .

In the case of dicyanoacetylene (NC_4N), the column density derived here for the protonated proxy is 1.1×10^{10} cm $^{-2}$. In this case there is also a metastable isomer which can be used as proxy, which is NC_3NC . This molecule is polar, with a calculated dipole moment of 1.11 D, and its rotational spectrum has been measured in the laboratory (Huckauf et al. 1999). At the current level of sensitivity of the QUIJOTE data, we did not detect this species, and derive a 3σ upper limit to its column density of 7.3×10^{10} cm $^{-2}$ assuming a rotational temperature of 7.5 K, in the middle of the range 5-10 K typically found in TMC-1. Therefore the abundance ratio $\text{NC}_3\text{NC}/\text{NC}_4\text{NH}^+$ in TMC-1 is < 7 , i.e., smaller than the ratio $\text{CNCN}/\text{NCCNH}^+$, which is ~ 9 . If the abundance ratios between the protonated and metastable proxies are not that different for NCCN and NC_4N , a deeper integration should lead to the detection of NC_3NC in TMC-1.

The formation of NCCNH^+ and NC_4NH^+ likely occurs by proton transfer to the neutral counterparts NCCN and NC_4N , respectively. Indeed both NCCN and NC_4N have high proton affinities, 674.7 kJ mol $^{-1}$ (Hunter & Lias 1998) and 736 kJ mol $^{-1}$ (Marcelino et al. 2020), respectively. The abundance ratio $\text{NCCNH}^+/\text{NCCN}$ was calculated to be $\sim 10^{-4}$ from a chemical model by Agúndez et al. (2015), although these authors noticed that the ratio may be closer to 10^{-3} because the chemical model underestimated by a factor of ~ 10 the protonated-to-neutral abundance ratios of related cyanides, such as HCN/HNC and

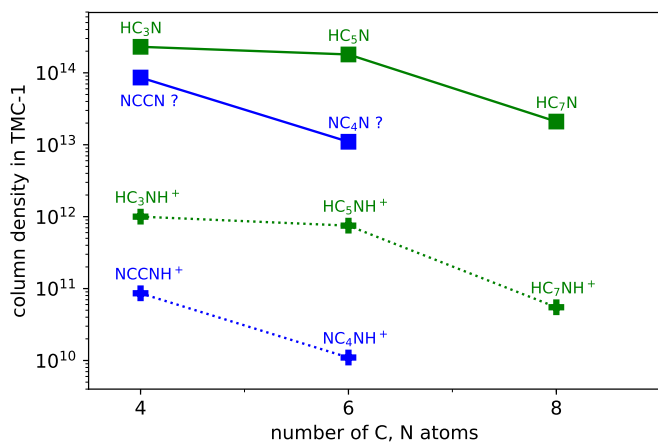


Fig. 4. Column densities in TMC-1 for monocyanopolyynes (in green) and dicyanopolyynes (in blue), and their protonated forms. Observed column densities are taken from Agúndez et al. (2015), Cernicharo et al. (2020a), Marcelino et al. (2020), Cabezas et al. (2022b), and this work. The column densities of NCCN and NC_4N are estimated from those of NCCNH^+ and NC_4NH^+ , respectively, assuming a protonated-to-neutral abundance ratio of 10^{-3} (see text).

HC_3N . From the detection of CNCN and arguments based on the expected similarity of the CNCN/NCCN and $\text{HCCNC}/\text{HCCCN}$ ratios, Agúndez et al. (2018) estimated the abundance of NCCN to be around 4.5×10^{-9} relative to H_2 , which is consistent with a $\text{NCCNH}^+/\text{NCCN}$ ratio of the order of 10^{-3} . The protonated-to-neutral abundance ratios derived from observations of cold dense clouds lie in the range 10^{-3} – 10^{-1} for neutral molecules with proton affinities larger than that of CO (Agúndez et al. 2022). For the monocyanopolyynes HC_3N , HC_5N , and HC_7N , the protonated-to-neutral abundance ratios are a few 10^{-3} . If we assume a protonated-to-neutral abundance ratio of 10^{-3} for NCCN and NC_4N , the estimated column densities of these dicyanopolyynes are somewhat lower, by factors of 3 and 15, than those of the corresponding monocyanopolyynes HC_3N and HC_5N (see Fig. 4). For the next member of the series of dicyanopolyynes, NC_6N , we can estimate its column density to be around $\sim 10^{12} \text{ cm}^{-2}$, assuming that the decrease in the column density with size found for HC_5N and HC_7N holds also for NC_4N and NC_6N (see Fig. 4). Assuming a protonated-to-neutral ratio of 10^{-3} , the column density of its protonated form, NC_6NH^+ , would be $\sim 10^9 \text{ cm}^{-2}$. According to the rotational constants and dipole moment calculated by Cabezas et al. (2022b), the most intense lines of NC_6NH^+ are expected to lie in the range 10–30 GHz, although the expected brightness temperatures are as low as 0.2 mK, which would require very sensitive observations.

Now the question is how are dicyanopolyynes formed in cold dense clouds. In the case of the simplest member of the series, NCCN, its formation is thought to occur by the reaction (Petrie et al. 2003)



Similarly, for NC_4N one can consider the reaction



If this reaction is the main source of NC_4N , we should expect the $\text{NC}_4\text{N}/\text{NCCN}$ ratio to reflect the $\text{C}_3\text{N}/\text{CN}$ ratio. In TMC-1 the $\text{C}_3\text{N}/\text{CN}$ ratio is 1.2 (Agúndez et al. in prep; Pratap et al. 1997), while the $\text{NC}_4\text{N}/\text{NCCN}$ ratio can be assumed to a first approximation to be given by the $\text{NC}_4\text{NH}^+/\text{NCCNH}^+$ ratio, which is

0.13. Given that C_3N is as abundant as CN in TMC-1, one should expect NC_4N to be as abundant as NCCN. From the observed abundances of NCCNH^+ and NC_4NH^+ , we infer that NC_4N is somewhat less abundant than NCCN, which could happen if the rate coefficient of reaction (2) is lower than that of reaction (1) or if NC_4N is destroyed more rapidly than NCCN. Other plausible reactions, such as,



are unlikely to be behind the formation of NC_4N in TMC-1 because the abundance ratios HNC_3/HNC and HCCNC/HNC are 0.002 and 0.011, respectively (Pratap et al. 1997; Cernicharo et al. 2020a), which are much lower than the inferred $\text{NC}_4\text{N}/\text{NCCN}$ ratio of 0.13.

5. Conclusions

We observed six harmonically related lines in our QUIJOTE line survey of TMC-1, which we identify as due to protonated dicyanoacetylene (NC_4NH^+). The detection of this species, together with the previous detections of NCCNH^+ and CNCN , support the hypothesis that dicyanopolyynes are abundant in cold dense clouds. We estimate that dicyanopolyynes are only a few times to one order of magnitude less abundant than their corresponding monocyanopolyynes.

Acknowledgements. We acknowledge funding support from Spanish Ministerio de Ciencia e Innovación through grants PID2019-106110GB-I00, PID2019-107115GB-C21, and PID2019-106235GB-I00 and from the European Research Council (ERC Grant 610256: NANOCOSMOS).

References

- Agúndez, M., Cernicharo, J., & Guélin, M. 2014, *A&A*, 570, A45
 Agúndez, M., Cernicharo, J., de Vicente, P., et al. 2015, *A&A*, 579, L10
 Agúndez, M., Marcelino, N., & Cernicharo, J. 2018, *ApJ*, 861, L22
 Agúndez, M., Cabezas, C., Marcelino, N., et al. 2022, *A&A*, 659, L9
 Cabezas, C., Agúndez, M., Marcelino, N., et al. 2021, *A&A*, 654, A45
 Cabezas, C., Agúndez, M., Marcelino, N., et al. 2022a, *A&A*, 657, L4
 Cabezas, C., Agúndez, M., Marcelino, N., et al. 2022b, *A&A*, 659, L8
 Cernicharo, J. 2012, in *European Conference on Laboratory Astrophysics*, eds. C. Stehlé, C. Joblin, & L. d’Hendecourt, *EAS Publication Series*, 58, 251
 Cernicharo, J., Marcelino, N., Agúndez, M., et al. 2020a, *A&A*, 642, L8
 Cernicharo, J., Marcelino, N., Agúndez, M., et al. 2020b, *A&A*, 642, L17
 Cernicharo, J., Cabezas, C., Endo, Y., et al. 2021a, *A&A*, 646, L3
 Cernicharo, J., Cabezas, C., Bailleux, S., et al. 2021b, *A&A*, 646, L7
 Cernicharo, J., Agúndez, M., Kaiser, R. I., et al. 2021c, *A&A*, 652, L9
 Cernicharo, J., Agúndez, M., Cabezas, C., et al. 2022a, *A&A*, 657, L16
 Cernicharo, J., Fuentetaja, R., Agúndez, M., et al. 2022b, *A&A*, 663, L9
 Coustenis, A., Bézar, B., Gautier, D., et al. 1991, *Icarus*, 89, 152
 Fossé, D., Cernicharo, J., Gerin, M., & Cox, P. 2001, *ApJ*, 552, 168
 Hänni, N., Altwegg, K., Balsiger, H., et al. 2021, *A&A*, 647, A22
 Huckauf, A., Guarnieri, A., Heyl, Å., et al. 1999, *Chem. Phys. Lett.*, 303, 607
 Hunter, E. P. L. & Lias, S. G. 1998, *J. Phys. Chem. Ref. Data*, 27, 413
 Jolly, A., Cottini, V., Fayt, A. et al. 2015, *Icarus*, 248, 340
 Kołos, R. & Grabowski, Z. R. 2000, *Ap&SS*, 271, 65
 Kunde, V. G., Aikin, A. C., Hanel, R. A., et al. 1981, *Nature*, 292, 292
 Marcelino, N., Agúndez, M., Tercero, B., et al. 2020, *A&A*, 643, L6
 Linke, R. A., Guélin, M., & Langer, W. D. 1983, *ApJ*, 271, L85
 Müller, H. S. P., Schlöder, F., Stutzki, J., & Winnewisser, G. 2005, *J. Mol. Struct.*, 742, 215
 Petrie, S., Millar, T. J., & Markwick, A. J. 2003, *MNRAS*, 341, 609
 Pickett, H. M., Poynter, R. L., Cohen, E. A., et al. 1998, *J. Quant. Spectr. Rad. Transfer*, 60, 883
 Pratap, P., Dickens, J. E., Snell, R. L., et al. 1997, *ApJ*, 486, 862
 Samuelson, R. E., Mayo, L. A., Knuckles, M. A., & Khanna, R. J. 1997, *Planet. Space Sci.*, 45, 941
 Sylvestre, M., Teanby, N. A., Dobrijevic, M., et al. 2020, *AJ*, 160, 178
 Tercero, F., López-Pérez, J. A., Gallego, J. D., et al. 2021, *A&A*, 645, A37
 Vastel, C., Loison, J.-C., Wakelam, V., & Lefloch, B. 2019, *A&A*, 625, A91